# STUDY ON IRON DISPERSION LAW AND CONTROL MEASURES OF DEAD-END BRANCH PIPE

**Jianxun Chen[1], Jinliang Gao[2], Wenyan Wu[3], Guanghui Wang[4], Qiang Ding[5],**

**Shihua Qi[6] and Bo Li[7]**

[1,2,7] School of Environment, Harbin Institute of Technology, Harbin, China
[3] School of Engineering and the Built Environment, Birmingham City University, Birmingham, UK
[4,5] Capital eco-pro group, Beijing, China
[6] Heilongjiang College of Construction, Harbin, China

[1] cjianxun877@gmail.com,   [2] gjl@hit.edu.cn, [3] wenyan.wu@bcu.ac.uk,
[4,5] 18292005003@163.com, [6] qishihua@126.com, [7] 2931907043@qq.com

## Abstract

The paper aims to investigate the dispersion law and mechanism of total iron from dead-end metal branch pipe to main pipe under the impact of hydraulic disturbance. A full scale experimental water distribution network including a transport main pipe as well as six dead-end branch was set up and computational-fluid-dynamics (CFD) simulation are adopted to study the dispersion phenomenon. The cavity flow theory is adopted to clarify the inner dispersion mechanism. Firstly, the CFD model is examined through the comparison of results between the two experimental methods under the same condition. Secondly, performing the effect of the Reynolds number in main pipe on the total dispersion concentration of iron. Thirdly, the characteristics of interaction between flow field and the inner mechanism linked to streamline map and concentration distribution map are analysed based on the concept of cavity flow. The future research content is briefly proposed.

**Keywords**
Dead-end branch pipe, iron dispersion, full scale distribution setup, computational-fluid-dynamics (CFD), cavity flow theory.

## 1    INTRODUCTION

The "red water" problem caused by the release of iron in the metal pipes has attracted much attention from users and water supply enterprises. Iron in cast iron pipes is released into water in the form of ions and compounds, which is the main reason for the phenomenon of "red water" [1]. Many scholars have carried out detailed research on the iron release model from different angles, and have achieved certain research results[2-4]. Most of them focus on static experiments, iron release and movement in the single and small diameter pipe. Full-scale model and the interaction influence between the pipe connections are scarce.

The existing water supply network is a complex network composed of looped and branched networks. The looped networks can not only ensure the reliability of water supply, but also improve the liquidity and avoid the generation of stagnant water. The branched pipes is mainly responsible for transferring and connecting users or water facilities. In terms of fluidity, the risk of water quality deterioration caused by branch pipes is significantly higher than that of looped pipes.

There are a large number of dead-end branch pipes in the water network due to the installation of valves, fire hydrants and other accessory equipment, and the water age in those pipes is too long and the dissolved oxygen concentration is significantly reduced, which will aggravate the iron release in the branch pipe wall. Under the condition of hydraulic disturbance and iron concentration gradient, soluble iron in the branch pipe will be released into the adjacent main pipe, which will seriously affect the water quality of the whole water supply system.

The branch pipe and the main pipe in the water supply network are usually connected by a tee fitting, forming a structure similar to a cavity at the connection. Cavity is a classical simplified physical model, which contains a large number of complex hydrodynamic problems, such as flow stability, vortex structure in cavity, coupling mechanism of flow and noise [5]. In water supply network, the connection between the main pipe and the dead-end branch pipe can be regarded as a typical cavity structure, which involves the shear layer instability of the cavity front, the generation and development of vortex, flow separation and other related physical processes. When the water in the main pipe flows through the cavity structure, the shear flow at the mouth of the cavity (that is, the connection between the main pipe and the branch pipe) interacts with the flow in the cavity (the water in the branch pipe), and the shear layer interacts with the cavity wall.  Severe pressure, velocity and other pulsations are generated, causing a series of complex flow phenomenon in the cavity[6]. The theory of cavity flow plays an important role in studying the mechanism of iron dispersion in dead-end branch pipes.

Based on cavity flow theory, this manuscript analyses the influence factors and mechanism of iron dispersion from dead-end branch pipe to main pipe by constructing a full-scale water supply pipeline experiment platform and using experimental device and computational fluid dynamics numerical analysis method. Combining with cavity flow theory, some suggestions are put forward for the control of iron dispersion process in branch pipe.

## 2    MATERIAL AND METHOD

### 2.1    The Construction of experimental device

The full-scale water distribution system experimental device is shown in Figure1. It was constructed with acrylonitrile butadiene styrene(ABS) pipe and the main diameter are DN200(the main pipe) and DN100(the dead-end branch pipe). The length of main pipe is 30m and branch pipe is 6m. The other main components including two isolated

**2022, Universitat Politècnica de València**
**2nd WDSA/CCWI Joint Conference**

stainless steel water tanks with the same volume of $2.25m^3$, a centrifugal pump with $Q_{max}=50m^3 \cdot h^{-1}$ and $H=32mH_2O$ controlled by a frequency converter, an ultrasonic flowmeter with measuring range from 0 to 100 $m^3 \cdot h^{-1}$, a pressure gauge with range from 0 to 0.6 MPa, nine butterfly valves(three of which are 100mm diameter and the rest are 200mm diameter). The device is arranged in a looped shape and all components are connected via flanges in order to facilitate modification and maintenance .

The function of the two tanks are water supply to all device and receive water from device, respectively. The water used during the experimental process is directly from the water tap in the laboratory. In order to control the length of dead-end branch pipe, the branch pipe is divided into six equal parts which are connected with butterfly valve and the length of all the parts is 1m. The length of branch pipe is depended on those valves' status. There are two ball valves are installed at both ends of one branch pipe (shown as in Fig1C) and one is used to exhaust air in the pipe and the other is used to fill the branch pipe with mixing water from the dosing tank placed near the branch pipe. The data of pump speed, flow and pressure are collected by automatic control system, and the collection frequency is 60HZ.

In the course of the experiment, the Reynold number of main pipe is controlled by adjusting frequency converter of pump. The diameter-length ratio(DLR) could be only controlled by open or close the valve in the branch pipe because the diameter of branch pipe is fixed. The concentration of iron solution is determined by controlled the ratio of iron quality and water added into dosing tank. After the completely mixing, the solution is pumped into the branch pipe through the beneath ball valve. When a set of experiments have completed, the full pipe must be flushed until the water is as clear as it was before the experiment. Through the above measure, the effect of residual iron on the experimental results can be reduced as much as possible. During the experiment, water samples were taken by the sampling ball valve at the front of the main pipe and at the branch pipe, and the iron concentration in the water samples were measured by ICP-MS (Inductively Coupled Plasma Mass Spectrometry).



*Figure 1. Full-scale water distribution system experimental device*

## 2.2　Simulation scheme setting

Three basic methods are utilised in this experimental research including device experiment, theoretical analysis based on model hypothesis and numerical simulation by solving mathematical equations to study the law of fluid motion. Computational fluid dynamics (CFD) is widely used in fluid research because it can reduce excessive

dependence on experimental devices, reduce experimental costs and improve experimental efficiency, significantly.  It has been used to the study of leakage characteristics and water quality mixing in junction of water supply network[7,8]. In this paper, the iron dispersion process in dead-end branch pipe is analysed by utilising the advantage of computational fluid dynamics in numerical solution and flow field analysis.

The iron dispersion phenomenon of dead-end branch follows the three conservation laws of mass, energy and momentum. In addition, as the dispersion process is involved, the component transport equation should also be considered. The above four equations can be solved simultaneously by computational fluid dynamics to obtain the distribution of iron in branch pipe and main pipe.

### 2.2.1 Model construction and parameter setting

In this paper, the tee fitting at the connection between the main pipe and the dead-end branch pipe is taken as the experimental object, and Creo-3D design software is used to establish the calculation model. The flow medium in the pipeline is set as water, and incompressible; A total of 9 geometric models with different branch length were established. The main pipe length, main pipe diameter and branch pipe diameter of all models were set to the same value, which pipe diameter are 1000mm, 200mm and 100mm. And the branch pipe length was set to 100mm, 300mm, 500mm, 700mm, 1000mm, 2000mm, 4000mm, 6000mm and 9000mm, respectively.

The left opening of the main pipe was taken as the inlet boundary, and the boundary condition was set as the velocity inlet. Parameters of the initial velocity, turbulence intensity and hydraulic diameter were set. The direction of velocity was perpendicular to the inlet boundary, and the inlet was defined as no pollutant concentration according to the actual situation. The right opening of the main pipe was taken as the outlet boundary, and the boundary condition was set as the pressure outlet. The inner wall of the pipe is set as non-slip static wall, and the wall is divided into the wall containing pollutants and the wall without pollutants. The initial mass fraction of iron is set on the wall containing pollutants to simulate the reaction between the pipe wall and the components in the bulk water and the continuous transport process of pollutants into the water. The branch pipe was divided into adaptive regions, and the initial concentration of pollutants in the branch pipe was set for local initialization. The model with branch pipe length of 500mm is shown in Figure 2.
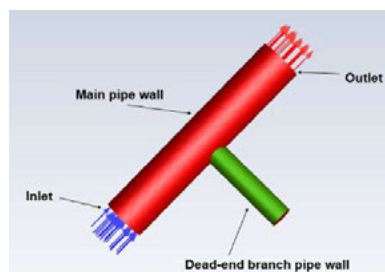


*Figure2. CFD model with branch pipe length of 500mm*

In order to solve the changes of flow field, velocity field and concentration field with time, transient analysis was selected, large eddy simulation (LES) was used as the turbulence solution model, and WALE was selected as the sublattice stress model. At the same time, the component transport was set up to build the iron dispersion model in the dead-end branch pipe. In the setting of the transient calculation solver, SIMPLEC algorithm was adopted as the pressure-velocity coupling algorithm, and First Order Implicit was taken as the transient discrete scheme. The spatial discrete scheme was the second-order upwind scheme. After setting the time step, step number and the maximum iterative step number within the unit step size, the iterative calculation was carried out.

### 2.2.2 Grid partitioning and independence verification

The ICEM software was adopted to grid the whole fluid area. The main flow area, velocity inlet and pressure outlet at the fluid area are encrypted. The inlet wall is encrypted from the left to the middle, while the outlet wall is encrypted in the opposite way. A total of five grid partitioning schemes with different density were set up. Except for differences in grid size and density, the five grids were all divided on the basis of model size corresponding to Figure 2, and other parameters were set the same. Grid size and quantity are shown in Table 1. Large eddy simulation was used to carry out numerical calculation for every grid scheme. The simulated initial total iron concentration in the branch pipe was set as $C_0=1mol/m^3$, the inlet flow rate was 0.8m/s, and the temperature is 300K. The variation of mass fraction of total iron at the main pipe outlet interface with time is shown in Figure 3.

*Table 1. Grid partitioning schemes*

| Schemes No | 1 | 2 | 3 | 4 | 5 |
|---|---|---|---|---|---|
| Grid quantity | 86187 | 134435 | 200320 | 259496 | 307436 |
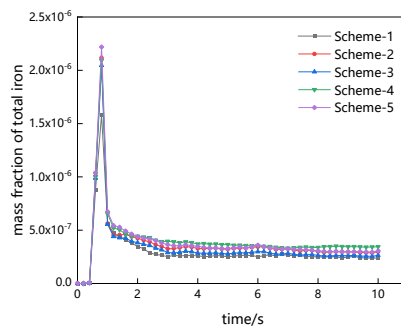


*Figure 3. Variation of mass fraction of total iron with time*

The variation trends of mass fraction of total iron at the outlet of different grid partitioning schemes are roughly the same, but there is a significant difference between the dispersion amount of peak and stable status for every scheme. The corresponding peak mass fraction of scheme-1 is higher than that of the other four schemes, but there is little gap with the four schemes after stability. It is speculated that the difference in the peak value is the main reason. In the stable stage of outlet mass fraction, there is no

significant difference in the variation trend and the value of mass fraction between scheme-2 and scheme-5, and the number of grids are 134435 and 307436 respectively. After comprehensive consideration of calculation accuracy and efficiency, scheme-2 was selected.

## 2.3 Mathematical model verification

The accuracy verification of the CFD numerical model is the premise to determine whether it can be used in subsequent research. It is an effective method to prove the reliability of the model by comparing the results of the experimental device and the numerical model under the same condition. The mass fraction of total iron at the main pipe outlet was selected as the validation index. If the absolute error between the two results was within 20%, it proved that the numerical model had certain accuracy and could be used in subsequent experiments. Otherwise, the model parameters need to be adjusted continuously until the error is less than 20%. This paper mainly studied the influence of three factors on iron dispersion in the dead-end branch pipe, so it is necessary to compare the index differences between two results under three different research variants to ensure the accuracy and reliability of the numerical model.

A total of 9 schemes are designed, as shown in Table 2. Among them, the influence of diameter-length ratio on iron dispersion was analysed in Row 1-4, the influence of Reynolds number was analysed in Row 5-7, and the influence of iron concentration in branch pipe was analysed in the other two schemes.

*Table 2. Schemes of mathematical model verification*

| Condition num | Length of branch pipe ( mm ) | Diameter of branch pipe ( mm ) | Ratio of diameter-length | Re of incoming flow | Initital iron concentration ( mol/m$^3$ ) |
|---|---|---|---|---|---|
| 1 | 1,000 | 100 | 0.100 | 20,000 | 8 |
| 2 | 1,000 | 100 | 0.100 | 28,000 | 8 |
| 3 | 1,000 | 100 | 0.100 | 32,000 | 8 |
| 4 | 1,000 | 100 | 0.100 | 20,000 | 1 |
| 5 | 1,000 | 100 | 0.100 | 20,000 | 2 |
| 6 | 1,000 | 100 | 0.100 | 20,000 | 4 |
| 7 | 2,000 | 100 | 0.050 | 20,000 | 8 |
| 8 | 4,000 | 100 | 0.025 | 20,000 | 8 |
| 9 | 6,000 | 100 | 0.017 | 20,000 | 8 |

## 2.4 Experimental scheme design

Based on the verified numerical model and its advantages in flow field analysis, several more detailed experimental scheme was designed to explore the mechanism of iron dispersion. Those schemes are shown in Table 3.

In all schemes, the diameter and length of the main pipe and the diameter of the dead-end branch pipe are kept 200mm, 1,000mm, 100mm respectively. The first nine schemes were designed to study the effect of DLR which is changed by adjusting the length of the branch pipe, the total iron concentration in the branch pipe was kept 1.0mol/m$^3$, and the main pipe Reynolds number was set as 200,000. The eight schemes (shown as Table 3) were designed to study the effect of main pipe Reynolds number by adjusting the flow rate of the main pipe. And the total iron concentration of the branch pipe and the length of the branch pipe are set 1.0mol/m$^3$ and 500mm.

*Table 3. Experimental scheme design*

| Scheme num | Length of branch pipe/mm | Ratio of diameter-length | Concentration of total iron in branch pipe(mol/m$^3$) | Re of main pipe |
|---|---|---|---|---|
| 1 | 500 | 0.200 | 1.0 | 2,000 |
| 2 | 500 | 0.200 | 1.0 | 6,000 |
| 3 | 500 | 0.200 | 1.0 | 12,000 |
| 4 | 500 | 0.200 | 1.0 | 20,000 |
| 5 | 500 | 0.200 | 1.0 | 80,000 |
| 6 | 500 | 0.200 | 1.0 | 160,000 |
| 7 | 500 | 0.200 | 1.0 | 240,000 |
| 8 | 500 | 0.200 | 1.0 | 360,000 |

## 3 RESULTS AND DISCUSSION

### 3.1 Model verification

The accuracy of the numerical model was studied according to the experimental scheme in Table 2. Due to the disturbance of water in the main pipe, iron dispersion in the dead-end branch pipe is a continuous process, and it takes a period of time to reach a stable status. In view of this, in the numerical model, the total iron concentration of the main pipe outlet selected the stabilized concentration; In the device experiment, water samples were taken from the downstream sampling location of the main pipe at an interval of 5 seconds, and the total iron concentration of outlet after stabilization was seen as the total iron concentration.

Figure 4 shows the total iron mass fraction and absolute error of main pipe outlet after stability obtained from numerical model and device experiment. Among the 9 experimental schemes, the total iron concentration obtained from numerical model is slightly higher than that of the device experiment. It is speculated that it is due to the disturbance of iron concentration in the dead-end branch pipe caused by the sudden opening of the dead-end branch pipe valve during the experimental operation. And the irregular shape of the fitting connection also affects the iron dispersion process. The absolute errors of the nine experiments are all less than 20%, which meet the numerical model validation conditions set in this paper, proving the applicability of parameter

setting to study the effects of three factors on iron dispersion. The subsequent studies were carried out on the basis of the parameter setting.
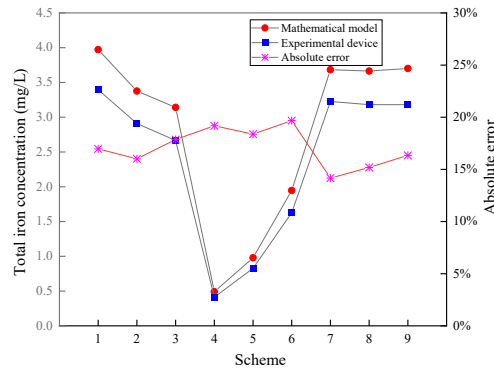


*Figure 4. Comparison for numerical model and device experiment result*

## 3.2    The effect of Reynolds number on iron dispersion

The variation rule of total iron mass fraction at the outlet with time under eight schemes obtained by large eddy simulation analysis is shown in Figure 5. Due to different flow rates, the time for dispersion to stabilization is also different. The stabilization time decreases from 200s to 2s when Reynolds number changes from 2000 to 360,000. And the larger the Reynolds number, the shorter the time required for the stabilization of the dispersion.
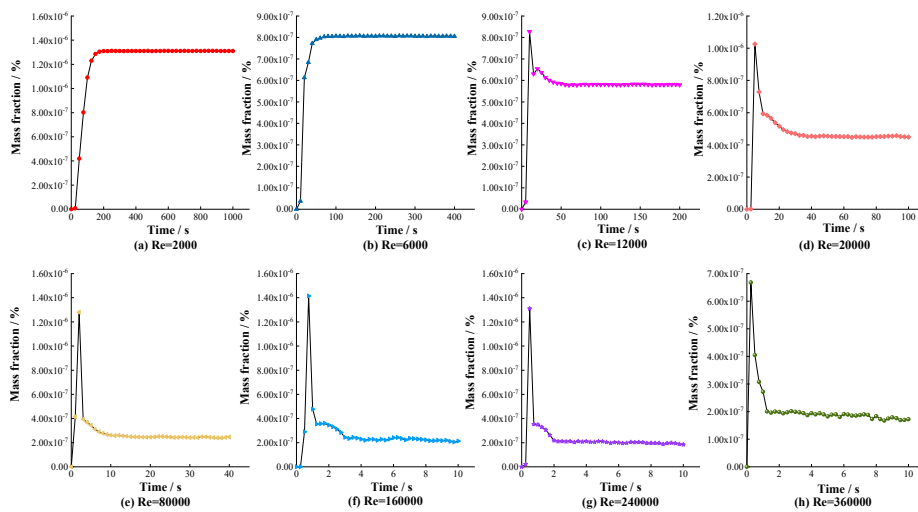


*Figure 5. Variation of total iron mass fraction with time under different Reynolds number*

Under the schemes of Re=2,000 and Re=6,000, the total iron mass fraction at the outlet increased firstly and then tended to be stable. When Re > 12,000, the fraction increased to the peak at first, then decreased gradually and maintained in a stable range. The scheme of Re=12,000 can be seen as a transition state from low Reynolds number to high Reynolds number. The main reasons for this phenomenon are as follows: when the water flow of the main pipe reaches the connection of the branch pipe under large Reynolds number, the main water containing pollutants in the branch pipe will be greatly disturbed. At this time, a large number of pollutants are included in the water of

the main pipe, and this part of water reaches the outlet of the main pipe, resulting in the peak value of the mass fraction of the total iron at the outlet. In the stable stage, only the outlet mass fraction of Re = 160,000, 240,000 and 360,000 fluctuated slightly, while the rest conditions remained constant.

The variation of peak value and stable value with Reynolds number is shown in Figure 6. When Re < 160,000, the maximum value of the total iron mass fraction at main pipe outlet increases gradually with the increase of Reynolds number. When Re = 160,000, the outlet mass fraction reaches the maximum value of $1.4×10^{-6}$. When Re > 160,000, the variation of maximum value of the mass fraction of total iron mass at export showed an opposite trend. When Re < 60,000, the Reynolds number has a significant effect on the outlet mass fraction. However, when Re > 60,000, the increase of Reynolds number has little effect on the outlet mass fraction at the outlet, and it always maintains around $2×10^{-7}$. It can be considered that under the condition of high Reynolds number, the change of Reynolds number has little influence on the total iron mass fraction at the outlet. The stable values and maximum values corresponding are equal for Re = 2000 and Re = 6000 respectively. While the maximum values of other Reynolds number are higher than the stable values. In order to facilitate subsequent analysis, Re = 2,000 and Re = 6,000 are referred to as low Reynolds number condition, Re = 12,000 is referred to as the transition status from low Reynolds number to high Reynolds number conditions, and Re > 12,000 is referred to as high Reynolds number conditions.
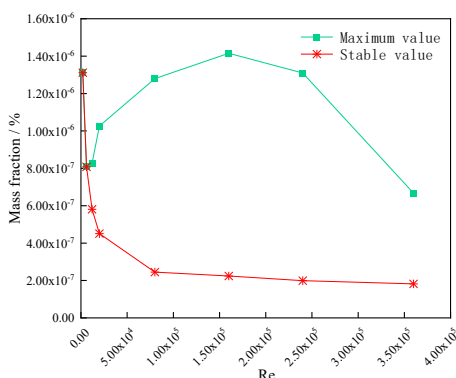


*Figure 6. The maximum and stable total iron mass fraction under different Reynolds number*

In order to explore the influence of different Reynolds numbers on iron dispersion, the maps of concentration distribution at three representative stages which including low Reynolds number stage (Re = 2,000), transition stage (Re = 12,000) and high Reynolds number stage (Re = 240,000), are selected for analysis, as shown in Figure 7.

It can be observed from Figure 7(a) that at the initial 5s of the flow, the concentration boundary at the junction of the branch pipe and the main pipe expands to the end of the branch pipe and the downstream of the main pipe, respectively. At 10s, more and more iron in the cavity diffuse from the downstream end of the cavity to the main pipe, and the concentration boundary in the branch pipe continues to expand to the end of the branch pipe. At 15s and 25s, the iron initially diffused into the main pipe continue to

move to the outlet, and the flow state and concentration boundary in the dead-end branch pipe remain stable; At 50s, the initially diffused iron reached the outlet, and the mass fraction at the outlet began to gradually increase with time; At 200s, the flow state in main pipe had been stabilized, and the mass fraction at the outlet have no change.

Figure 7(b) is the map of the concentration distribution in the transition stage (Re = 12,000). There are obvious differences between Re = 12,000 and Re = 2,000 in terms of the concentration peak and the dispersion state. In the initial stage, i.e. at t=1s, the main body water of the main pipe disturbs the distribution of iron in the branch pipes, which is more severe than that of the low Reynolds number, and the occurrence time is earlier. At 4s, due to the initial fluctuation taking away part of the pollutants, a vortex with concentration gradient is generated downstream of the cavity. The iron diffused in the initial stage moves to the outlet of the main pipe, and the dispersion amount of iron gradually decreases in at the later stage; At 8s, the iron generated by the strong disturbance reaches the outlet, forming a concentration peak, and the concentration boundary in the dead-end branch pipe continuously extends to the end of the branch pipe. At 17s, the low-concentration boundary at the end of the branch pipe extends to the maximum, but the iron concentration in the boundary center gradually increases, and the iron flowing out from the downstream end of the cavity tend to be stable along the pipe wall. At 21 s and 40 s, the concentration boundary in the branch pipe gradually decreases, but the concentration gradually increases. At this time, the concentration distribution change and the pollutant dispersion amount are relatively stable for both main and branch pipe. And this is called the stable dispersion stage.

Figure 7(c) shows the map of the concentration distribution under high Reynolds number (Re = 240,000). The concentration distribution in the high Reynolds number stage changes obviously. At 0.1s, a severe disturbance occurred at the connection between the branch pipe and the main pipe. Under the action of such a fluctuation, a relatively large number of iron were diffused from the back edge of the cavity, and the iron at the boundary flowed out, forming an upward convex low concentration zone in the branch pipe. At 0.2s, the low concentration band formed at the initial stage gradually became larger and extended to the end of the branch pipe, and the fraction of the band central was at a lower value. The initially diffused pollutants moved along the pipe wall to the main pipe outlet along with the main body water of the main pipe. At 0.5s, the low concentration band in the branch pipe moved along the branch pipe wall to the end of the branch pipe, and the band range continued to increase. At this time, the iron diffused in the initial stage reached the outlet of the main pipe, which corresponds to the peak concentration in Figure 6. At 0.7s and 1.6s, the amount of iron flowing out from the branch pipe to the main pipe has been stabilized. It can be clearly observed that the content of pollutants corresponding to the pipe wall of the main pipe downstream of the cavity is very small, and the mass fraction of the outlet is less than $1.5 \times 10^{-5}$. The low concentration zone in the branch pipe extended anticlockwise to the middle of the branch pipe and continued to extend. At 2.5s, the low concentration zone in the branch pipe splited into two concentration zones, and the low concentration gradient in the

center of the concentration zone almost disappears. At this moment, the concentration of pollutants close to the main pipe wall remains constant and is in a stable stage.
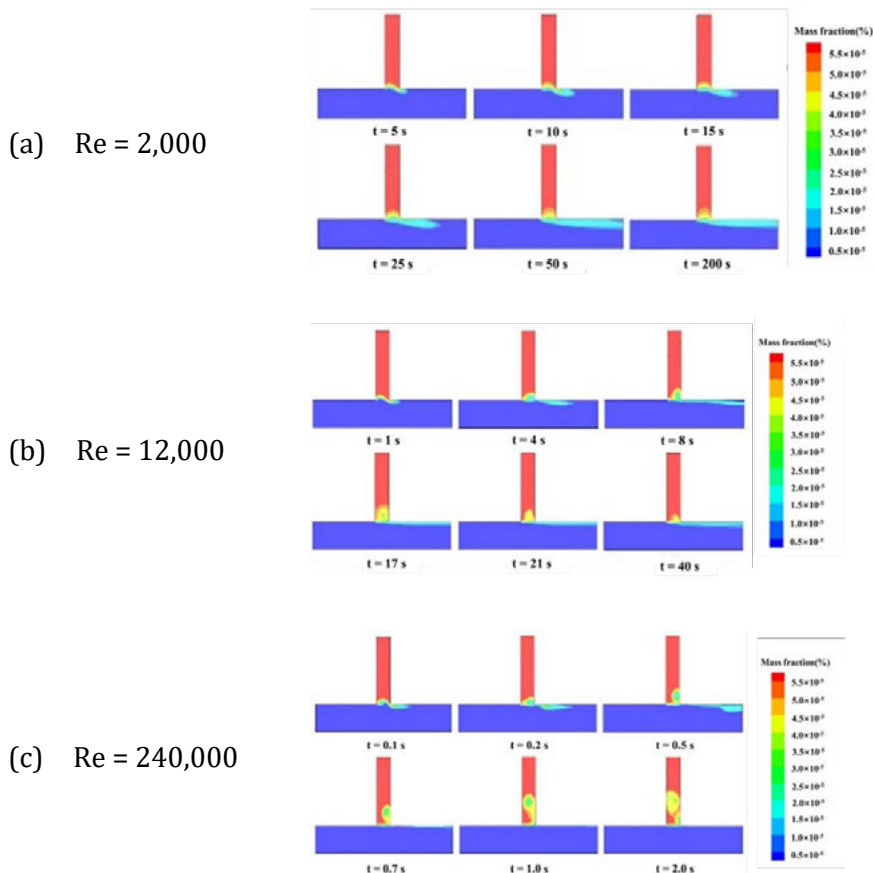


*Figure 7. Concentration distribution map under different Reynolds number*

## 3.3    Mechanism analysis

From the above analysis, DLR, iron concentration in branch pipe and incoming Reynolds number are three influencing factors for iron dispersion in dead-end branch. The main influence on the flow field characteristics is the incoming Reynolds number. Under different Reynolds numbers, the flow field characteristics of dead-end branch pipe are mainly divided into low Reynolds number stage and high Reynolds number stage. In this paper, two representative conditions are selected for flow field characteristics analysis, in which Re = 6,000 at low Reynolds number stage and Re = 160,000 at high Reynolds number stage.

### 3.3.1    Lower Reynold
In order to analyse the relationship among the dispersion amount, the concentration distribution and the characteristics of the flow field, the instantaneous flow field analysis was carried out by combining the instantaneous streamline diagram and the corresponding concentration distribution map. Figure 8 shows the streamlines and concentration distributions at low Reynolds numbers of 2s, 6s, and 16s.

As can be seen from Figure 8 (a) that at the initial stage of flow (t=2s), when the water flow of the main pipe passes through the dead-end branch pipe, the boundary layer is lifted, and the streamline diagram is shown as an upward convex curve. It can be seen from the track and direction of the streamline that water in main pipe enters the branch pipe. The free shear layer colliders with the back wall of the branch at the middle of the branch pipe, resulting in the separation of the shear layer. A part of the separated shear layer flows back to the front edge of the cavity and forms a small vortex structure on the front edge of the cavity and the back wall of the cavity, and the other part leaves the dead-end branch from the rear edge of the cavity. Affected by the uplift of the boundary layer, the iron in the branch pipe diffuse into the main pipe.

Figure 8(b) shows the streamline diagram and concentration distribution diagram at t=6s. At this time, the large vortex developed in the branch pipe stably exists in the middle of the cavity, and the streamline state at the wall of the main pipe downstream of the branch pipe is stable. There is only one large backflow area in the branch pipe. From the concentration distribution map, it can be seen that the concentration gradient range at the front end of the branch pipe caused by the backflow area of the branch pipe gradually extends. The concentration gradient area in the main pipe gradually widens and lengthens.

The streamline and concentration distribution diagram at t=16s are shown in Figure 8(c). At this time, the cavity flow field has reached a steady state in the dead-end branch under the low Reynolds number state. There are two vortices stably in the dead end branch pipe, the vortex near the main pipe is the main vortex, and the vortex direction is counterclockwise. From the map of the concentration distribution, it can be seen that the distribution of the entire concentration gradient is highly coincident with the main vortex, indicating that the dispersion of iron is closely related to the main vortex. There is also a secondary vortex in the depth of the dead-end branch, which is driven by the main vortex and generated in a clockwise direction, so that the iron concentration in the depth of the dead-end branch pipe can be transported to the outlet of the branch. At this time, the concentration gradient range in the branch pipe continues to intensify, and the concentration gradient range in the main pipe becomes longer and narrower.

Based on the above analysis, it can be concluded that the flow field at low Reynolds number is relatively stable, the boundary layer is deeply depressed towards the end of the branch pipe. And the free shear layer collides with the back wall of the branch pipe, which affects the vortex structure of the flow field. The concentration distribution is closely related to the change of the vortex structure. The change of the streamline map also directly reflects the change of the concentration distribution map. The final concentration gradient range coincides with the height of the main vortex, and the main vortex never breaks away from the shear layer in position, indicating that the amount of iron dispersion is closely related to the main vortex.

(a)  t = 2s          (b)  t = 6s          (c)  t = 16s
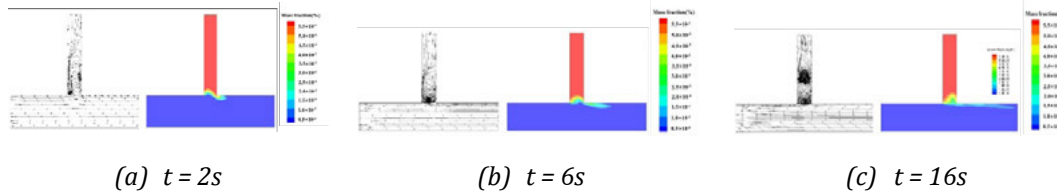
*Figure 8. streamline map and concentration distribution map under different time at lower Re*

### 3.3.2   Higher Reynold

The instantaneous flow diagram and the corresponding concentration distribution map are used to analyse the instantaneous flow field at the stage of high Reynolds number. By comparing the flow field characteristics at low Reynolds number, the relationship between dispersion trend, concentration distribution and flow field characteristics is summarized. The streamline diagrams and concentration distribution map at the Reynolds number of 0.1s, 0.4s, 2.1s and 4s are shown as Figure 9.



( a ) t=0.1s          (b) t=0.4s

(c) t=2.1s          (d)  t=4s
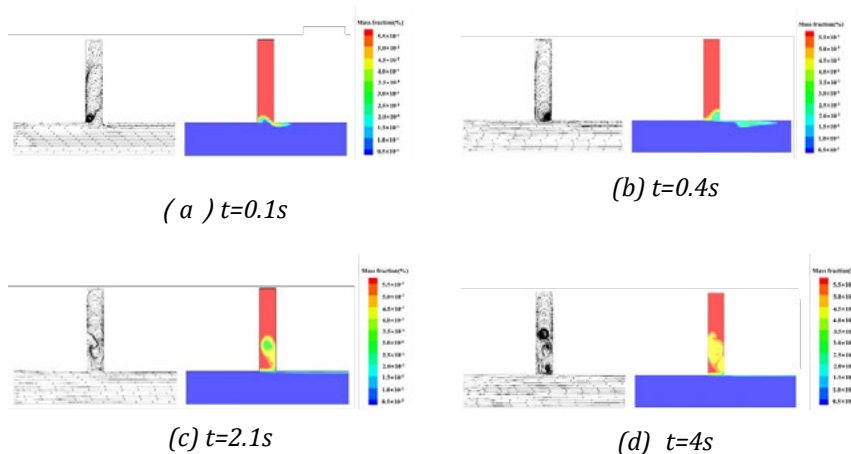
*Figure 9. Streamline map and concentration distribution map under different time at higher Re*

By analysing the streamline diagram and concentration distribution map under high Reynolds number, it can be found that the flow field under high Reynolds number is not as stable as that at low Reynolds number. A significant difference occurred when the main vortex collided with the trailing edge of the cavity and moved away from the boundary to the depth of the branch. The splitting of vortices and the generation of new vortices occur during the movement. And finally form two secondary vortices and a primary vortex at the trailing edge of the cavity.

The overall flow field is characterized by the formation and development of vortexes in the shear layer, the collision and shedding of vortexes with the back edge of the cavity, the splitting of vortexes and the generation of new vortexes, and finally the three vortexes form a set of stable vortex structures.

The iron dispersion trend and concentration distribution in the dead-end branch pipe are closely related to the development process of the vortex structure, which is embodied in the form of low concentration range in the concentration distribution map.

The vortex development process includes the formation, development, collision and shedding of the low concentration range, and the final concentration range and center concentration increase with the movement and splitting of the vortex structure.

## 4    CONCLUSION

In this paper, the iron dispersion law of the connection between the main pipe and the dead-end branch pipe is analysed and the dispersion mechanism was studied on the basis of the concept of cavity. The mathematical model of dead-end branch iron dispersion was established by combining computational fluid dynamics numerical simulation with device experiments, and an experimental platform for dead-end branch iron dispersion was designed and built to verify the accuracy of the numerical model. The law of iron dispersion in dead-end branch pipe under different Reynolds number of inlet flow was analysed, and the iron dispersion mechanism at the connection between dead-end branch pipe and main pipe was clarified.

The numerical model was used to simulate the iron dispersion in the dead-end branch pipe under different Reynolds numbers of incoming flow. In the low Reynolds number stage, the dispersion amount first increased and then stabilized, and the dispersion amount of iron was large. The high Reynolds number stage has less dispersion after stabilization.

Combined with the theory of cavity flow, the flow field characteristics of the iron dispersion in the dead-end branch pipe are studied. At the low Reynolds number stage, the flow field characteristics were concluded as follows: the formation, development and shedding of the leading edge vortex of the cavity, which stabilized in the middle of the cavity, and finally a second-order vortex was generated along the depth of the dead-end branch pipe. The high Reynolds number stage is characterized by the formation and development of vortices in the shear layer, the collision and shedding, the splitting of vortices and the generation of new vortices, and finally the three vortices form a group of stable vortices structure. The concentration distribution is highly coincident with the vortex structure, including the formation, development, collision, shedding of the low concentration range, the final concentration range and the central concentration increasing with the movement and splitting of the vortex structure.

Future studies will combine the flow control method of the cavity to explore the dispersion mode, control mechanism and the controllable effect of iron dispersion in the blind-end branch pipe by adding the new fitting in main pipe.

## 5    REFERENCES

[1]  SETH A, BACHMANN R, BOXALL J, et al. Characterisation of materials causing discolouration in potable water systems [J]. Water Science and Technology, 2004, 49(2): 27-32.

[2]  BENSON A S, DIETRICH A M, GALLAGHER D L. Evaluation of Iron Release Models for Water Distribution Systems [J]. Critical Reviews in Environmental Science and Technology, 2012, 42(1): 44-97.

[3] Shahra Essa and Wenyan Wu (2020) Water contaminants detection using sensor placement approach in smart water networks, Journal of Ambient Intelligence and Humanized Computing (2020), https://doi.org/10.1007/s12652-020-02262-x, Springer 25 June 2020.

[4] Jinliang Gao, Shiyuan Hu, Wenyan Wu, et al. Experiment and Simulation of Ferrous Ions Diffusion at the Dead-end Branch Pipes of Water Distribution System, 1st WDSA/CCWI 2018 Joint Conference, Kingston, Ontario, Canada – July 23-25, 2018.

[5] SHAMEKHI A, SADEGHY K. Cavity flow simulation of Carreau-Yasuda non-Newtonian fluids using PIM meshfree method [J]. Applied Mathematical Modelling, 2009, 33(11): 4131-45.

[6] DE ROECK W, RUBIO G, BAELMANS M, et al. Toward accurate hybrid prediction techniques for cavity flow noise applications [J]. International Journal for Numerical Methods in Fluids, 2009, 61(12): 1363-87.

[7] CASSA A M, VAN ZYL J E. Predicting the head-leakage slope of cracks in pipes subject to elastic deformations [J]. Journal of Water Supply Research and Technology-Aqua, 2013, 62(4): 214-23.

[8] Webb, S. W., and B. G. Van Bloemen Waanders. 2007. "High fidelity computational fluid dynamics for mixing in water distribution systems." In Proc., 8th Annual Water Distribution Systems Analysis Symp. 2006, 154. Reston, VA: ASCE

## 6   ACKNOWLEDGMENTS